

Statistical Properties of Galactic Starlight Polarization

Pablo Fosalba^{1,4}, Alex Lazarian², Simon Prunet³, Jan A. Tauber⁴

ABSTRACT

We present a statistical analysis of Galactic interstellar polarization from the largest compilation available of starlight data. The data comprises ~ 9300 stars of which we have selected ~ 5500 for our analysis. We find a nearly linear growth of mean polarization degree with extinction. The amplitude of this correlation shows that interstellar grains are not fully aligned with the Galactic magnetic field, which can be interpreted as the effect of a large random component of the field. In agreement with earlier studies of more limited scope, we estimate the ratio of the uniform to the random plane-of-the-sky components of the magnetic field to be $\mathbf{B}_u/\mathbf{B}_r \approx 0.8$. Moreover, a clear correlation exists between polarization degree and polarization angle what provides evidence that the magnetic field geometry follows Galactic structures on large-scales.

The angular power spectrum C_ℓ of the starlight polarization degree for Galactic plane data ($|b| < 10^\circ$) is consistent with a power-law, $C_\ell \propto \ell^{-1.5}$ (where $\ell \sim 180^\circ/\theta$ is the multipole order), for all angular scales $\theta \gtrsim 10'$. An investigation of sparse and inhomogeneous sampling of the data indicates that, in the entire range of scales probed, the starlight data analyzed traces an underlying continuum polarized emission in the visible with the same angular power spectrum. Our findings suggest that starlight data can be safely used for the modeling of Galactic polarized continuum emission at other wavelengths.

Subject headings: dust, extinction — polarization — Galaxy: stellar content, structure — methods: statistical

¹Institut d’Astrophysique de Paris, 98bis Boulevard Arago, F-75014 Paris, France; E-mail: fosalba@iap.fr

²Department of Astronomy, University of Wisconsin, Madison, USA; E-mail: lazarian@dante.astro.wisc.edu

³Canadian Institute for Theoretical Astrophysics, McLennan Labs 60 St George Street, Toronto ON M5S 3H8, Canada; E-mail: prunet@cita.utoronto.ca

⁴Astrophysics Division, SSD of ESA-ESTEC, P.O. Box 299, NL-2200 AG Noordwijk, The Netherlands; E-mail: jtauber@astro.estec.esa.nl

1. Introduction

The large scale emission from the Milky Way at radio, mm-wave and far-infrared wavelengths is known to be polarized (see e.g, de Oliveira-Costa & Tegmark 1999). The underlying common cause is the Galactic magnetic field, though the particular polarization mechanism is wavelength-dependent. It ranges from the synchrotron emission process which is the driving mechanism at long wavelengths to the absorption/emission properties of aligned dust grains which are expected to account for the short-wavelength emission. Therefore the measurement of the polarized Galactic emission should yield valuable information on our Galaxy's magnetic field (see e.g, Zweibel & Heiles 1997, Hildebrand et al 2000, Heitsch et al 2001). In particular, starlight polarization vectors trace the plane-of-the-sky projection of the Galactic magnetic field (Zweibel & Heiles 1997) and measurements of polarization for stars of different distances reveals the 3D distribution of magnetic field orientations averaged along the line of sight.

However currently the only available large scale maps of polarized Galactic emission are at low (radio) frequencies (i.e, $\nu \leq 2.7$ GHz, see Tucci et al 2000, for a description of available data), where the Galactic signature is significantly distorted by (relatively) local Faraday rotation effects. At far-infrared and mm wavelengths, measurements have been made of a few very small regions, largely dense dark clouds, mainly concentrated in the Galactic plane (Hildebrand et al 1999, Novak et al 2000; see also Hildebrand et al 2000, Heitsch et al 2001, for recent reviews) but they reflect only rather local distortions of the large-scale magnetic field. Therefore, within this wavelength range, the only large scale view has been obtained by observation of and analogy with external spiral galaxies similar to our own (Zweibel & Heiles 1997).

The next generation of Cosmic Microwave background (CMB) missions (i.e. MAP - <http://map.gsfc.nasa.gov/> - and Planck - <http://astro.estec.esa.nl/Planck>) will fill this gap by providing polarization measurements of the whole sky at mm wavelengths. For these missions, the polarized Galactic dust emission is primarily a nuisance which has to be removed from the underlying cosmic signal (see Prunet & Lazarian 1999, Draine & Lazarian 1999, Lazarian 2001), but in so doing they will also provide for the first time the means to map the Galactic magnetic field. Planck in particular covers a range of wavelengths (1 cm to 300 μ m) in which different polarization mechanisms are dominant, which will provide powerful means to uncover the common underlying magnetic field distribution.

At optical wavelengths, there do exist many measurements of starlight polarization (Appenzeller 1974, Schroeder 1976, Mathewson et al 1978, Markkanen 1979, Krautter 1980, Korhonen & Reiz 1986, Bel et al 1993, Leroy 1993, Berdyugin et al 1995, Reiz & Franco 1998). Observed starlight polarization is believed to be caused by selective absorption by magnetically aligned interstellar dust grains along the line of sight; because these measurements are limited by dust extinction, they give us a view of the behavior of the magnetic field only in a local bubble around us. Furthermore, the pencil-beam nature of these observations means that the view afforded is punctual, with a sampling that is both inhomogeneous and sparse. However, analysis

of compilations of such measurements (see Heiles 2000 and references therein) imply that they do contain information about both the large-scale and the random components of the Galactic field in the vicinity of the Sun. Therefore it is useful to extract as much information as possible from this data.

In this paper we analyze the most complete compilation to date of optical polarization observations. This analysis will allow us to extract basic information on the large scale statistical properties of the polarization field in the visible. We do this by studying the correlations between stellar parameters and computing the angular power spectrum (a convenient statistical estimator for analyzing 2D full-sky maps) of the optical polarization degree from Milky Way stars; in so doing we investigate the systematic effects introduced by the sparse and inhomogeneous sampling which is intrinsic to starlight measurements.

The outline of the paper is as follows: §2 presents the starlight data analyzed. We describe the distribution of the sources in §3 and study their correlations as a function of distance and Galactic coordinate in §4. We compute the angular power spectrum of starlight polarization degree in §5. We finish with a discussion of our results in §6.

2. Data

The starlight polarization data used in this analysis is taken from the compilation by Heiles 2000. This compilation includes data from 9286 sources taken from a dozen of catalogs, combining multiple observations, providing accurate positions and reliable estimates for extinction and distance of stars.

From this catalog, we have selected a subsample of 5513 stars (60% of the data) based on the following criteria:

- the degree and angle of polarization are given
- small error in the polarization degree ($< 0.25\%$)
- a (positive) extinction is given

Note that the most constraining requirement is the last one (extinction): if this requirement were not used, the subsample would include 8280 stars (90 % of the whole compilation). However we need to include the degree of extinction in the visible as it strongly correlates with the polarization degree (see §4 below) and it is a basic ingredient to model dust polarization at other wavelengths (Hildebrand & Dragovan 1995). We shall present this analysis in a forthcoming paper (Fosalba et al 2001). All the stars in the Heiles compilation fulfilling the above requirements also have quoted distance (with an estimated 20 % error for most of the sources, see Heiles 2000).

3. Distribution of Sources

Fig 1 shows the distribution of sources in our subsample for data binned in Galactic coordinates (top panel) as well as in distance and latitude (bottom panel). As shown in the latter, all high latitude ($|b| > 10^\circ$) stars are nearby ($d < 1$ Kpc). Within the Galactic plane one can find relatively distant stars, though the vast majority are within 2 Kpc. Thus, this is clearly a local sample.

This is also seen in Table 1, which summarizes the mean stellar parameters (i.e, polarization degree $P(\%)$ and extinction as measured by the color excess $E(B-V)$) in the subsample as a function of latitude and distance. Note that in Table 1, high latitude (low latitude) means $|b| > 10^\circ$ ($|b| < 10^\circ$) and nearby (distant) denotes $d < 1$ Kpc ($d > 1$ Kpc). The quantities between brackets denote amount % of all stars in the sample. Low-latitude stars have large values of the polarization degree $P(\%) \approx 1.7$, and extinction $E(B-V) \approx 0.5$, while high-latitude sources exhibit significantly lower values, $P(\%) \approx 0.5$, $E(B-V) \approx 0.15$. Polarization vectors are typically oriented along the galactic plane ($\theta_p \approx 90^\circ$) although a more detailed analysis reveals a rich spatial distribution (see Fig 11 and §4 below).

Histograms displaying the distribution of sources with Galactic latitude b , distance d , polarization degree $P(\%)$ and extinction $E(B-V)$ bins, are given in Fig 2.

4. Correlations between Stellar Parameters

Light emitted from stars is assumed to be unpolarized; the observed polarization from starlight is believed to result from extinction by interstellar dust grains along the line of sight to the observer. Thus, for a homogeneous distribution of intervening dust, the larger the path-length starlight travels to reach the observer, the larger the polarization degree and extinction are expected to be. According to this simple picture, Galactic regions with low polarization degree (and extinction) trace nearby stars, while regions with high values of the polarization degree (and extinction) correspond to distant stars. This is actually observed in the sample of Starlight data, as shown in Figs 9 & 10, where nearby stars (light green sources) are mainly at high Galactic latitudes, while distant stars (red-purple sources) are found in the Galactic plane (see also Table 1 for mean values of the stellar parameters). In particular, the spatial distribution of both parameters in Galactic coordinates is expected to be highly correlated and this is clearly observed in Figs 9 & 10.

We describe in detail below how the stellar parameters which describe the sources in the subsample correlate with one another and what information can be extracted from the behavior found.

4.1. Behavior with Distance

The distribution of the polarization degree and extinction as a function of distance (average quantities in linear distance bins) for the sources considered are shown in Fig 3. It is seen that both stellar parameters grow linearly (to a good approximation) with distance up to $d \approx 2$ Kpc. Beyond ~ 2 Kpc, stars have roughly constant values for both quantities, i.e, $P(\%) \approx 2$, $E(B-V) \approx 0.6$. The overall behavior of $P(\%)$ and $E(B-V)$ with distance (in Kpc) can be best-fitted by third-order polynomials up to $d \approx 6$ Kpc(see Fig 3):

$$P(\%) \approx 0.13 + 1.81d - 0.47d^2 + 0.036d^3, \quad (1)$$

$$E(B-V) \approx 0.08 + 0.5d - 0.135d^2 + 0.0104d^3. \quad (2)$$

The similar behavior of both stellar parameters with distance already suggests a simple linear correlation (for data averaged in distance bins) between polarization degree and extinction. This is the case indeed as shown in Fig 4. The observed roughly linear correlation for individual sources is in agreement with measurements at $2.2 \mu\text{m}$ (Jones 1989) & $100 \mu\text{m}$ (Hildebrand et al 1995).

However the observed mean correlation amplitude for data averaged in extinction bins is much smaller than what is expected from interstellar dust grains completely aligned under a purely regular (no random component) external magnetic field $P(\%) \approx 9 E(B-V)$. This is also observed in the K-filter at $2.2 \mu\text{m}$ (Jones 1989). What is more, we find a slight deviation from the simple linear correlation,

$$P(\%) \approx 3.5 E(B-V)^{0.8}, \quad (3)$$

as displayed in the lower panel of Fig 4. In fact, this deviation from the linear correlation shows a similar dependence with extinction for K-band observations at $2.2 \mu\text{m}$, i.e, $P_k \approx 0.83 E(B-V)^{0.75}$ (Jones 1989). Eq(3) implies that the ratio of the observed to the optimal polarization degree,

$$\frac{P_{\text{Obs}}}{P_{\text{Max}}} \approx 0.39 E(B-V)^{-0.2} \quad (4)$$

This is, at least, a factor of 2 larger than the same ratio found for the K-filter at $2.2 \mu\text{m}$, $P_{\text{Obs}}/P_{\text{Max}} \approx 0.19$ (Jones 1989).

Next we study the dependence of the stellar parameters with Galactic coordinate.

4.2. Behavior with Galactic Longitude

In order to study the dependence of stellar parameters with Galactic longitude we have averaged the data in 10° longitude bins. As shown in Fig 5, both the polarization degree and the Stokes Q parameter, defined as $Q = \cos 2(\theta_p - 90^\circ)$ (θ_p is the polarization angle), exhibit, on average, a sinusoidal-like dependence with longitude with a 180° periodicity, well-fitted by the expressions,

$$P(\%) \approx 1.3 + 0.9 \sin(2l + 180^\circ), \quad (5)$$

$$Q \approx 0.4 + 0.5 \sin(2l + 100^\circ). \quad (6)$$

For Galactic longitudes $l \approx 50^\circ$ and $l \approx 230^\circ$ we find minimum values of Q, i.e, the stellar polarization vectors are orthogonal to the Galactic plane, $\theta_p \approx 0^\circ, 180^\circ$. Note that, at the Galactic plane, these directions approximately intersect the Cygnus-Orion spiral arm which suggests that, on average, polarization vectors do not align with this Galactic structure. Moreover, we also find minimum values of the polarization degree (or extinction as they are linearly correlated) for these Galactic longitudes. Approximately along these directions (as one moves away from the Galactic plane) one finds the edge of a supernova remnant, the spherical shell of Loop I (see red sources in Fig 11). Thus, a possible explanation for the values of the stellar parameters along these directions is that exploding supernovae in the Scorpius/Ophiuchus star cluster centered at $l \approx 0^\circ$, $b \approx 20^\circ$ (see Zweibel & Heiles 1997) could cause polarization vectors to be strongly aligned with the Galactic structure left by the supernova remnant.

On the other hand, maximum values of the polarization degree and Stokes Q parameter are found at $l \approx 140^\circ$ and $l \approx 320^\circ$, where the polarization vectors of dust grains are parallel to the Galactic disk structure, $\theta_p \approx 90^\circ$ (see light-green sources in Fig 11).

We note that the results shown in the lower panel of Fig 5 for the longitude dependence of the Stokes Q parameter are in good agreement with the analysis presented in Whittet (1992) for about 1000 nearby Galactic plane stars ($d < 0.6$ Kpc, $|b| < 3^\circ$).

4.3. Behavior with Galactic Latitude

As discussed in §3, most of the sources in our subsample are in the Galactic disk (75 % of the stars are found at $|b| < 10^\circ$, see Table 1). However, there is a statistically significant fraction of the sources at high Galactic latitudes (25 % of sources at $|b| > 10^\circ$) which allow us to investigate the mean variation of the correlations between stellar parameters as a function of latitude. For this purpose we have averaged the data in 10° (linear) latitude bins.

We find that the polarization degree shows a strong dependence with latitude as shown in the upper panel of Fig 6. Indeed, the behavior can be well described by a co-secant law:

$$P(\%) \approx 0.1 + 0.0067 \csc(0.05 |b|). \quad (7)$$

The Stokes Q parameter seems to correlate with the polarization degree in the Galactic plane alone (see the two highest data points in lower panel of Fig 6). This appears to indicate that the starlight polarization angles tend to be aligned with the Galactic plane structure ($\theta_p \approx 90^\circ$). However, the statistical significance in the measurement of the Stokes Q parameter (i.e, the polarization angle) is low at high latitudes given the lack of available data and the large degree of dispersion in the polarization angle (as large as 35-55 %, depending on latitude and distance; see also the large scatter in lower panel of Fig 5). Therefore it is hard to draw any conclusions about the correlation between the polarization degree and Stokes Q parameter on high Galactic latitudes from the current analysis.

5. The Angular Power Spectrum of the Starlight Polarization Degree

In this section, we analyze the starlight polarization data described in §2 to see whether and if so, to what extent, it traces from a statistical point of view the large-scale Galactic polarized continuum emission at visual wavelengths.

For this purpose we estimate the angular power spectrum of the starlight polarization degree (see Fig 9). The angular power spectrum is the convenient full-sky generalization of the 2D Fourier power spectrum, as the latter is only strictly valid in small (flat) patches of the sky. In particular, given a full-sky map of a scalar field S (such as the starlight polarization degree field) one can decompose it in on the spherical harmonic basis $Y_{\ell m}$ at any point (θ, ϕ) in the sky:

$$S(\theta, \phi) = \sum_{\ell m} a_{\ell m} Y_{\ell m}(\theta, \phi) \quad (8)$$

where the $a_{\ell m}$ are the coefficients of the projection of the 3D scalar field on the spherical harmonic basis and they fully determine the statistical properties of a Gaussian distributed field. The angular power spectrum is thus defined as a quadratic average of a given $a_{\ell m}$ coefficient over different m -modes:

$$C_\ell = \frac{1}{2\ell + 1} \sum_{m=-\ell}^{m=\ell} |a_{\ell m}|^2 \quad (9)$$

where C_ℓ estimates autocorrelations of the field at an angular scale $\theta \approx 180^\circ/\ell$, being ℓ the so-called multipole order. In a fully-sampled map, the two-point correlation function $\xi(\theta)$ of the scalar field S is simply related to the angular power spectrum:

$$\xi(\theta) = \langle S(\mathbf{q}_1) S(\mathbf{q}_2) \rangle = \sum_\ell \frac{\ell + 1/2}{\ell(\ell + 1)} C_\ell P_\ell(\cos \theta) \quad (10)$$

where $\cos \theta = \mathbf{q}_1 \cdot \mathbf{q}_2$ is the dot product of two unit vectors pointing to any pair of sky pixels, P_ℓ is the Legendre polynomial of multipole order ℓ and $\langle \dots \rangle$ denotes ensemble average.

Although the angular power spectrum C_ℓ is a straightforward statistic to calculate, its computation is usually limited to fully-sampled maps. As such, it conveys information at all angular

scales down to the map resolution. Note that for the starlight data, a map of very large spatial resolution is required as the information is essentially point-like. Furthermore significant systematic effects are expected to be introduced by the very sparse and inhomogeneous (clustered) nature of this data sample.

5.1. Power Spectrum Estimation of the Real Data

We want to assess to what extent the discrete data available on starlight polarization is able to trace an underlying polarized continuum emission in the visible. This problem is a particular case of a more general one, say, what information about the (large-scale) continuum emission can be extracted from sparse in-homogeneously distributed discrete data.

In order to address this issue, we shall investigate how the latter effects affect the angular power spectrum (PS) estimation. For this purpose, we have analyzed the Galactic plane data ($|b| < 10^\circ$), which is the most densely sampled in the catalog and therefore it is expected to yield the most reliable statistics.

5.1.1. Rough Harmonic Analysis

We aim at computing the PS of the starlight polarization degree data according to Eq(9). In order to do so, we have generated a full-sky map (we use a HEALPix tessellation, see <http://www.eso.org/kgorski/healpix>) for stars at $|b| < 10^\circ$, which comprises 4114 stars, i.e, non-zero pixels (see Table 1). The resolution of the map has been chosen to be high enough (3.5' pixels) so that different sources are not identified with the same pixel. The PS of this map, shown in Fig(7) (see green line), has been computed using the *anafast* program of the HEALPix package. The slope of the PS is well-fitted by $C_\ell \propto \ell^{-1.5}$ down to $\ell \lesssim 100$ which translates into angular scales $\theta \gtrsim 2^\circ$. On smaller scales $\theta \lesssim 2^\circ$, the PS is dominated by a flat shot-noise-like spectrum ($C_\ell = \text{constant}$), which is due to the effect of the large number of quasi-randomly located zero-valued pixels in the map, and which prevents us from measuring the PS of the underlying continuum signal down to the pixel resolution scale.

5.1.2. Improved Analysis: the Correlation Function Approach

In order to improve the simple analysis presented above, we should correct the data for the pixel window and the shot-noise intrinsic to the sparsely distributed data we want to analyze.

For this purpose we first compute the two-point correlation function of the polarization degree data using a quadratic estimator where the weighting is effectively done in pixel space (Szapudi & Szalay 1998; see also Szapudi et al 2001). The method consists of the following steps:

- Compute the correlation function $\xi(\theta)$ of the data on a very fine grid of θ (typically 300000 bins).
- Resample the grid at the roots of the Legendre polynomial of order ℓ_{max} , where ℓ_{max} is the maximum multipole at which one wishes to estimate the PS. The re-sampling, using a Gaussian interpolating kernel on the fine bins, weighted by the number of pairs per bin, is at the core of the method (see Szapudi et al 2001 for details).
- Obtain the PS by a simple Gauss-Legendre quadrature integration. The output is presented as flat band powers i.e, data averaged in multipole bins of width $\Delta\ell = 20$.

The advantage of this method (with respect to the Harmonic approach) is that it gives an unbiased estimate of the power spectrum for an arbitrary sampling of the sky, thus avoiding the shot-noise power bias that is visible in the traditional PS estimator, as given by Eq(9). In turn this typically translates into a noisy estimate for the range of ℓ 's where the shot-noise power dominates.

Fig 7 (see blue line) shows how this method allows for an efficient way of de-convolving the window function⁵ and removing the shot-noise component of the signal down to $\ell \approx 1000$, i.e, $\theta \approx 10'$ which is close to the map resolution $\theta \approx 3.5'$. Although the estimated signal is rather noisy on small scales $\ell \gtrsim 100$, where the shot-noise dominates, the PS can be well-fitted on average by a power-law $C_l \propto \ell^{-1.5}$ in the whole range of scales measured, $\ell \lesssim 1000$.

5.2. Power Spectrum Estimation of the Simulated Data

We would like to know how robust are the results obtained in the previous section. In particular, how sensitive is the estimated PS slope to the spatial distribution of stars used ? how does the clustering of the sources affect the PS analysis ? To answer these questions we have first simulated a *mock starlight map* in the Galactic plane ($|b| < 10^\circ$) for which we have computed the PS, as follows:

⁵This is effectively taken into account at a later stage, in multipole space, where C_ℓ is divided by the square of the pixel window function

- Generate a random-Gaussian realization full-sky map of a $C_\ell \approx \ell^{-1.5}$ (with arbitrary amplitude), using the *synfast* program of the HEALPix package, with the same spatial resolution than the original starlight data map (3.5' pixels). The latter PS gives a good fit to the starlight polarization degree PS for $\ell \lesssim 1000$, as shown in §5.1.
- Set all pixels outside the Galactic plane $|b| < 10^\circ$ to zero.
- Remove at random all but 4114 of the Galactic plane (3.5') pixels (or lines of sight) from the map. This leaves as many non-zero pixels from the random-Gaussian realization as in the original starlight data map (see Table 1).
- Compute the PS of the resulting sparsely sampled *mock starlight map* for the polarization degree as we did for the actual data according to the methods presented in §5.1.

As seen in Fig 8 (see green line), the rough harmonic analysis (see §5.1.1) shows that the simulated starlight data has approximately the same PS than the underlying densely sampled (effectively continuous) distributed data (red line) for multipoles $\ell \lesssim 40$ i.e, scales $\theta \gtrsim 5^\circ$. On smaller scales, shot-noise dominates the signal. However, the improved analysis based on the correlation function approach (see §5.1.2) allows to measure the PS of the underlying continuous distributed map from the sparsely sampled *mock starlight map* down to much higher multipoles, $\ell \lesssim 1000$ i.e, scales $\theta \gtrsim 10'$ (see green line), although the signal is rather noisy beyond the shot-noise dominance scale $\ell \sim 40$.

5.3. Effect of Clustering

Since the *mock starlight map* was generated from a random-Gaussian realization, we can compare the PS analysis obtained from it (see §5.2) to the one performed on the real data (see §5.1), which are clearly non-Gaussian distributed (see Fig 9), to see what is the effect of clustering or non-Gaussianity in the distribution of the lines of sight.

Our findings in §5.2 show that the clustering of the sources in the analyzed starlight polarization degree map shifts the scale where shot-noise dominates from $\theta \approx 5^\circ$ down to $\theta \approx 2^\circ$. Therefore, a rough harmonic analysis allows a clean measurement of the PS of the underlying continuously distributed map down to much (a factor of 2.5) smaller scales when the sources are strongly clustered. However, using the *improved* correlation function analysis, shot-noise and pixel window effects can be effectively removed down to approximately the map resolution scale (3.5') with hardly any dependence on the clustering of the sources. The price to pay for this is that the more clustered the sources are, the noisier the measured PS turns out to be on small scales (see blue lines in Figs §7 & 8).

6. Discussion

In this paper we present an statistical analysis of the largest compilation available of Galactic starlight polarization data. The data analyzed consists of 5513 stars, a large fraction of which is found at low Galactic latitudes ($|b| < 10^\circ$) and in the vicinity of the sun ($d < 1$ Kpc). Despite the inhomogeneous distribution of the sample, it allows for a proper statistical investigation of the large-scale behavior of the stellar parameters, such as the linear polarization (polarization degree and angle) and extinction, as induced by intervening dust grains.

The correlations between stellar parameters give some valuable information on the geometry and degree of uniformity of the Galactic magnetic field, as we discuss in §6.1 & §6.2. On the other hand, we discuss to what extent starlight data traces the the large-scale properties of the diffuse Galactic polarized emission in §6.3, based on our PS analysis (see §5.1).

6.1. Polarization Angle and Magnetic Field Orientation

Although no consensus has been reached in relation to what mechanism is the dominant in the interstellar environment⁶ (see discussion in Lazarian 2000) it is generally accepted that grains in diffuse interstellar gas tend to be aligned with their major axes perpendicular to the magnetic field. The cases where the alignment is suspected to be parallel to magnetic field are extremely rare (see Rao et al 1998) and can be safely ignored in our analysis.

According to this picture, the electric field of radiation transmitted by an interstellar dust grain is less absorbed along the grain minor axis and therefore polarized in that direction which is parallel to the external magnetic field orientation. Therefore, polarized starlight radiation vectors are oriented parallel to the Galactic magnetic field.

Since starlight polarization vectors are only seen as projected in the plane of the sky, they just give us direct information on the plane-of-the-sky projection of the Galactic magnetic field orientation. In §4.2 we found a strong alignment of starlight polarization vectors with the Galactic plane structures and the spherical shell of Loop 1 (see §4.2 & §4.3), which in turn provides evidence that *there is a net alignment of the magnetic field (as seen from its plane-of-the-sky projection) with Galactic structures on large-scales*.

However, we stress that the full reconstruction of the 3D magnetic field orientations (and strength) requires additional complementary data from radio (synchrotron), sub-mm/IR (dust) observations and rotational measures from distant pulsars (Zweibel & Heiles 1997).

⁶Radiative torque mechanism looks the most promising right now (Draine & Weingartner 1996, Draine & Weingartner 1997).

6.2. Polarization Degree and Efficiency of Magnetic Field Alignment

We have shown in our analysis that the starlight polarization degree and extinction are clearly correlated and on the mean, this correlation has a lower amplitude than what is expected from complete dust-grain alignment from homogeneous magnetic fields (see §4.1).

The fact that starlight data exhibits a lower polarization degree as a function of extinction than the theoretical upper limit, suggests that *either the grain alignment is not optimal or the Galactic magnetic field has a significant random component*.

For grains in clouds with high extinction the alignment tends to fail (Lazarian et al 1997) but our sample does not deal with such clouds. At the same time, measurements of high degree of polarization suggest that the alignment can be sufficiently efficient. Substantial variations of the grain properties (e.g, the degree of elongation) do not look promising either.

On the other hand, a random component of the magnetic field \mathbf{B}_r smears to some degree the correlation introduced by the uniform component \mathbf{B}_u (Jones 1989). This smearing effect is likely to affect the observed stars as supported by the high degree of incoherence (randomness) observed for the starlight polarization angle (see Fig 11). In what follows we shall assume that the latter is the dominant misalignment effect to infer an upper limit in the degree of randomness of the Galactic magnetic field.

It is well-known that, by assuming a model, one can relate the observed polarization degree to the ratio of uniform to random plane-of-the-sky components of the underlying magnetic field (see e.g, Heiles 1996). In particular, assuming Burn's model (Burn 1966), one finds for the starlight sample, Eq(4),

$$\frac{P_{\text{Obs}}}{P_{\text{Max}}} = \frac{\mathbf{B}_u^2}{\mathbf{B}_u^2 + \mathbf{B}_r^2} \approx 0.39 - 0.62 \quad (11)$$

within the range, $0.1 \lesssim E(B-V) \lesssim 1$, where the power-law is a good fit to $P_{\text{Obs}}/P_{\text{Max}}$ indeed. This yields, $\mathbf{B}_u/\mathbf{B}_r \approx 0.80 - 1.27$ for the same range. Note that Burn's model assumes a 3D distribution of the random component (consistent with a scenario with a uniform field distorted by supernovae explosions) and a long enough path-length for every line of sight i.e, a large number of intervening clouds. In fact, for a subsample of nearby stars, the model tends to overestimate the $\mathbf{B}_u/\mathbf{B}_r$ ratio (Heiles 1996). Note that this bias is actually consistent with Eq(4) which predicts a larger $P_{\text{Obs}}/P_{\text{Max}}$ for low extinction (or distance) and therefore, a larger $\mathbf{B}_u/\mathbf{B}_r$ ratio.

According to the above discussion, we take the value for high extinction $E(B-V) \gtrsim 1$, which corresponds to distant stars ($d > 1$ Kpc, see lower panel of Fig 3), as an unbiased estimate of the ratio, $\mathbf{B}_u/\mathbf{B}_r \approx 0.8$. This value is roughly consistent with previous estimates from starlight data (see Heiles 1996 for a review and references therein): $\mathbf{B}_u/\mathbf{B}_r \approx 0.68$. Note that $\mathbf{B}_u/\mathbf{B}_r$ as derived from starlight polarization data is typically larger than estimates from synchrotron polarization, $\mathbf{B}_u/\mathbf{B}_r \approx 0.54$, and it is significantly larger than that obtained from rotational measures of distant pulsars, $\mathbf{B}_u/\mathbf{B}_r \approx 0.28$.

The discrepancy between estimates from different data sets can be explained as every data set basically samples a different component of the interstellar medium: pulsars mainly trace the warm ionized medium, starlight data samples primarily the neutral media⁷ while synchrotron data seems to sample all components (Heiles 1996).

6.3. Large-scale Polarized Diffuse Emission

We have performed an angular power spectrum (PS) analysis of the starlight polarization degree. We have focused on Galactic plane data ($|b| < 10^\circ$) as it concentrates most of the sources in the sample and therefore makes the statistical analysis more reliable. Our analysis shows that the starlight polarization degree PS is well fitted by a power-law behavior, $C_\ell \propto \ell^{-1.5}$ for $\ell \lesssim 1000$ (where the multipole order $\ell \approx 180^\circ/\theta$) which translates into angular scales $\theta \gtrsim 10'$. This is approximately the pixel resolution scale used, $3.5'$ (see §5.1). This result was obtained thanks to a correlation function method which efficiently removes the shot-noise and pixel window effects that strongly affect the data on small scales (see §5.1.2).

We have assessed how the above results are affected by the *clustering* or non-Gaussianity in the distribution of sources by simulating a *mock starlight map* for the polarization degree (see §5.3). We found that the efficiency with which one measures the PS of the underlying densely-sampled signal is not significantly altered by the clustering of the sources, although for the real non-Gaussian distributed sources shot-noise dominates at smaller scales and the estimated PS is noisier than the simulated random-Gaussian case.

The above results provide evidence that the starlight data available in the galactic plane traces an underlying continuum emission in the visible with the same PS, $C_\ell \propto \ell^{-1.5}$, for scales $\ell \lesssim 1000$ ($\theta \gtrsim 10'$).

On the other hand, it is remarkable that the measured starlight polarization degree PS in the galactic plane $C_\ell \propto \ell^{-1.5}$ is consistent with recent estimates of the PS of Galactic synchrotron polarized diffuse emission at radio wavelengths at the same latitudes (Tucci et al 2000, Baccigalupi et al 2000), in the same range of scales, $\ell \lesssim 1000$. This might be an indication that, at least for low latitudes, the PS of Galactic polarized emission does not change significantly with wavelength.

The lack of starlight data on high-galactic latitudes does not allow to make a reliable measurement of the PS for the moment. In particular, it remains to be seen whether the PS slope varies significantly for high-galactic latitudes as recent analyses from synchrotron emission indicate (Baccigalupi et al 2000).

⁷HI dominates the column density, although H+ also contributes significantly (see Draine & Lazarian 1998).

In a forthcoming paper (Fosalba et al 2001), we shall use our results on starlight data to model Galactic polarized dust emission at sub-mm/FIR wavelengths and its effect on the process of foreground subtraction in CMB experiments.

We acknowledge the use of the starlight data compilation by C. Heiles who has kindly made it publicly available. PF is supported by a CMBNET fellowship of the European Comission.

REFERENCES

Appenzeller I., 1974, A&A, 36, 99

Baccigalupi C., Burigana C., Perrotta F., De Zotti G., La Porta L., Maino D., Maris M., Paladini R., 2000, A&A, in Press [astro-ph/0009135]

Bel N., Lafon J.-P.J., Leroy J.L., 1993, A&A, 270, 444

Berdyugin A., Snare M.-O., Teerikorpi P., 1995, A&A, 294, 568

Burn B.J., MNRAS, 1966, 133, 67

de Oliveira-Costa A., Tegmark M., (eds) 1999, “Microwave Foregrounds”, ASP, V181

Draine B.T., Lazarian A.L., 1998, ApJ, 494, L19

Draine B.T., Lazarian A.L., 1999, in “Microwave Foregrounds” eds. A. de Oliveira-Costa and M. Tegmark, ASP, V181, 133

Draine B.T., Lee H.M., 1984, ApJ, 285, 89

Draine B.T., Weingartner J.C., 1996, ApJ, 470, 551

Draine B.T., Weingartner J.C., 1997 ApJ, 480, 633

Fosalba P., et al. 2001, in preparation

Heiles C., 1996, ASP, in “Polarimetry of the Interstellar Medium” eds. W.G. Roberge and D.C.B. Whittet, V97, 457

Heiles, C., 2000, AJ, 119, 923
The data is publicly available by anonymous ftp at vermi.berkeley.edu. See pol15.out (compilation of data), and pol1.ps (description and references for the compiled data) in directory pub/polcat . It has also been recently made available through the web-sites:
<http://vizier.u-strasbg.fr/viz-bin/VizieR?-source=II/226>
<http://adc.gsfc.nasa.gov/viz-bin/VizieR?-source=II/226>
However, note that in these http addresses, no starlight extinction information is provided.

Heitsch F., Zweibel E.G., Mac Low, M-M., Li, P.S., Norman, M.L., 2001, ApJ, in Press [astro-ph/0103286]

Hildebrand R.H., Dotson J.L., Dowell C.D., Platt S.R., Schleuning D., Davidson J.A., Novak G., 1995, in “Airborne Astronomy Symposium on the Galactic Ecosystem: From Gas to Stars to Dust”, ASP, V73, 97

Hildebrand R.H., Dragovan M., 1995, ApJ, 450, 663

Hildebrand R.H., Dotson J.L., Dowell C.D., Schleuning D.A., Vaillancourt J.E., 1999, ApJ, 516, 834

Hildebrand R.H., Davidson J.A., Dotson J.L., Dowell C.D., Novak G., Vaillancourt J. E., 2000, PASP, 112, 1215

Jones T.J., 1989, ApJ, 346, 728

Korhonen T., Reiz A., 1986, A&A, 64, 487

Krautter J., 1980, A&AS, 39, 167

Lazarian A., Goodman A., Myers P. 1997, ApJ, 490, 273

Lazarian A., 2000, in “Cosmic Evolution and Galaxy Formation”, ASP, eds. J. Franco, E. Terlevich, O. Lopez-Cruz, I. Arétxaga, V215, 69, [astro-ph/0003314]

Lazarian A., 2001, astro-ph/0101001

Leroy J.L., 1993, A&A, 274, 203

Markkanen T., 1979, A&A, 74, 201

Mathewson D.S., Ford V.I., Klare G., Neckel T., Krautter J., 1978, Bull. Inf. CDS, 14, 115

Novak G., Dotson J.L., Dowell C.D., Hildebrand, R.H., Renbarger T., Schleuning, D.A., 2000, ApJ, 529, 241

Prunet S., Lazarian A., 1999, in “Microwave Foregrounds” eds. A. de Oliveira-Costa and M. Tegmark, ASP, V181, 113

Reiz A., Franco G.A.P., 1998, A&AS, 130, 133

Rao R., Crutcher R.M., Plambeck R.L., Wright M.C.H., 1998, ApJ, 502, L75

Schroeder R., 1976, A&AS, 23, 125

Szapudi I., Szalay A.S., 1998, ApJ, 494, L41

Szapudi I., Prunet S., Pogosyan D., Szalay A.S. Bond J.R., 2001, ApJ, 548, L115

Tucci M., Carretti E., Cecchini S., Fabri R., Orsini M., Pierpaoli E., 2000, NA, 5, 181

Whittet D.C.B., 1992, “Dust in the Galactic Environment”, IOP Publishing, London.

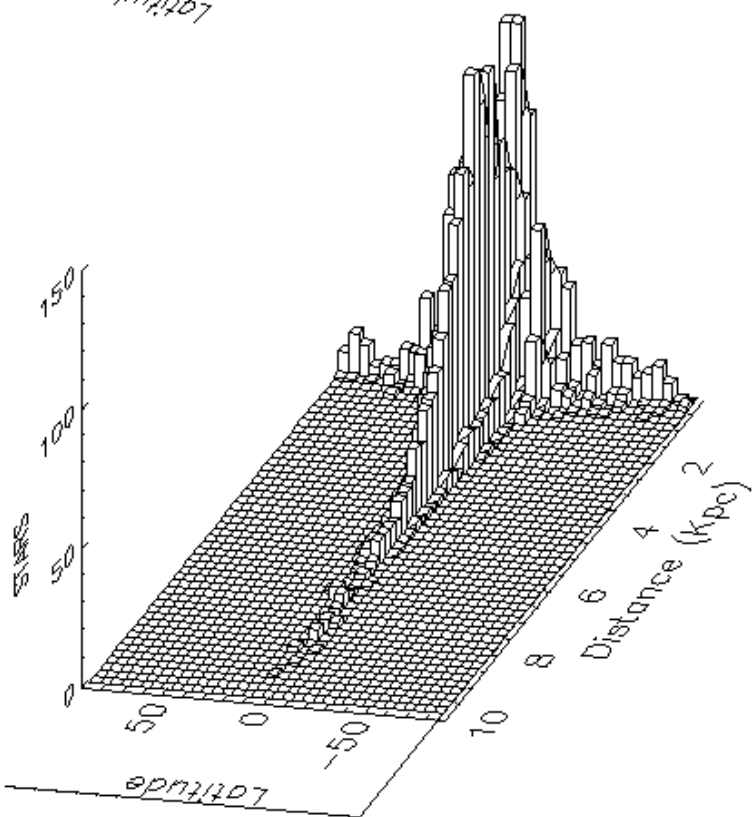
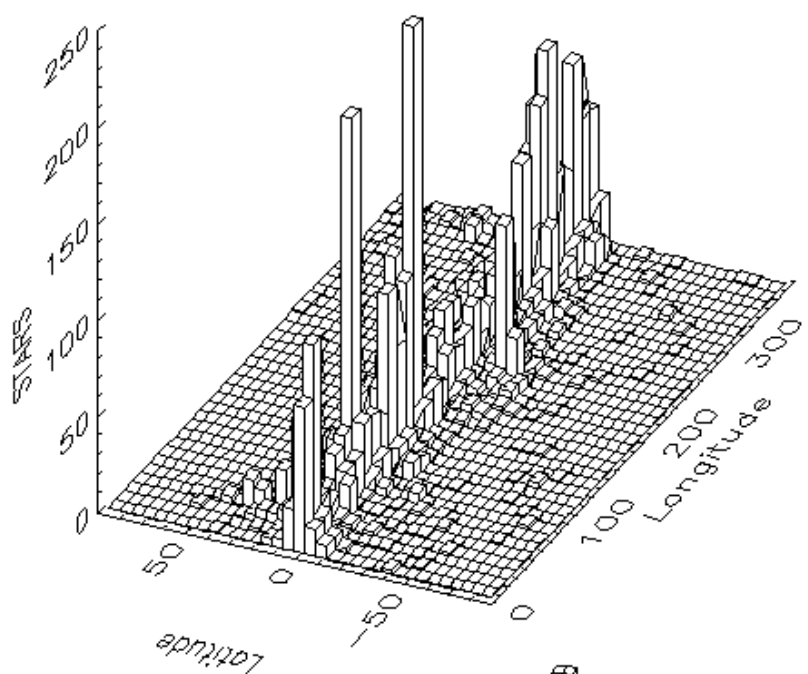
Zweibel E.G., Heiles C., 1997, Nature, 235, 131

Table 1. Mean Stellar Parameters: Sample of 5513 Stars

Latitude	Distance	Stars (%)	P(%)	E(B-V)	θ_p
Low latitude	Total	4114(75)	1.69	0.49	88.1
	Nearby	1451(26)	0.94	0.29	90.4
	Distant	2663(48)	2.09	0.60	86.9
High Latitude	Total	1399(25)	0.45	0.15	93.0
	Nearby	1315(24)	0.42	0.14	93.4
	Distant	84(1)	0.89	0.26	86.7

Note. — Mean stellar parameters i.e, polarization degree P(%), extinction E(B-V), and polarization angle θ_p , for the sample of 5513 stars analyzed, as a function of latitude and distance. High latitude (low latitude) means $|b| > 10^\circ$ ($|b| < 10^\circ$) and nearby (distant) denotes $d < 1$ Kpc ($d > 1$ Kpc).

Distribution of Sources (5513 Stars)



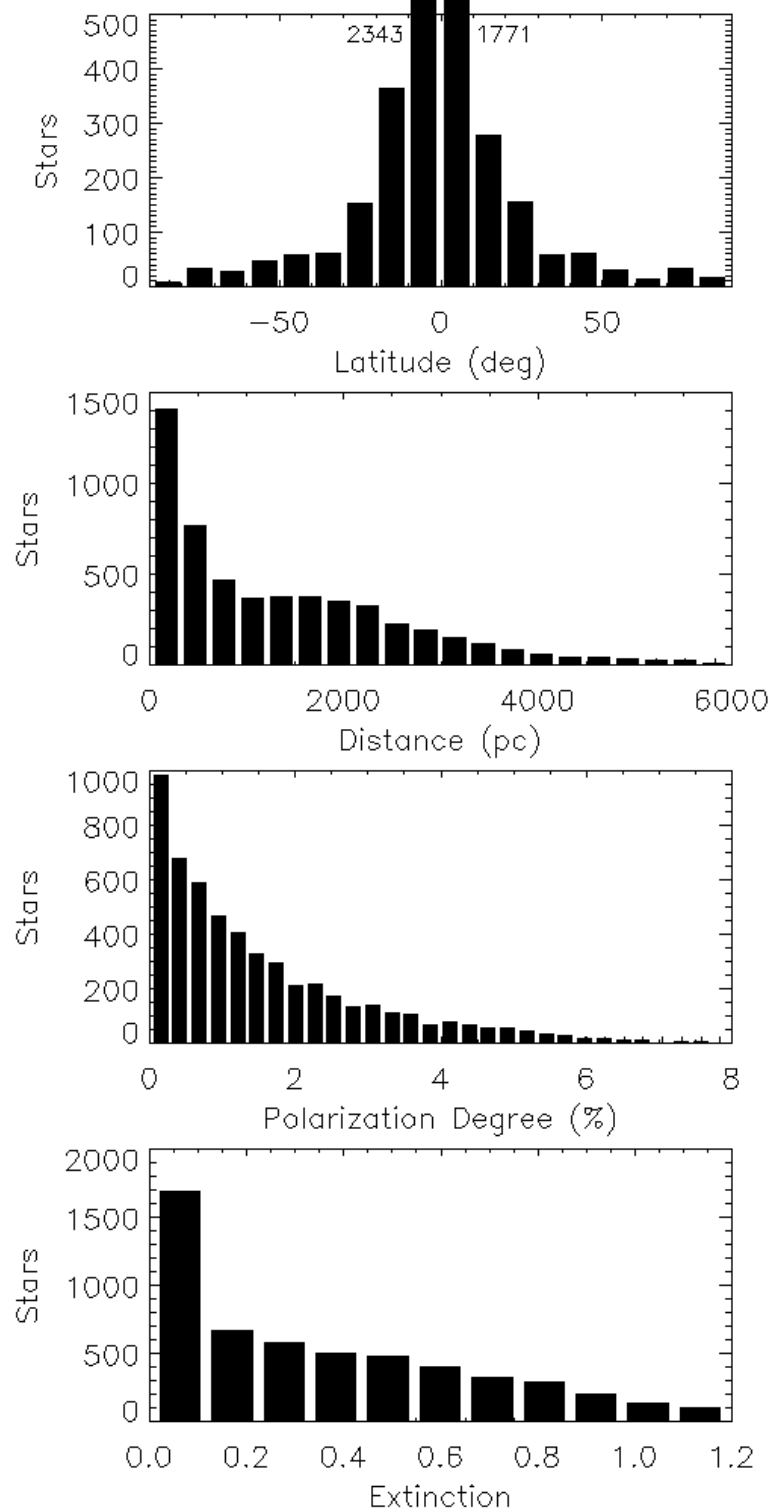


Fig. 2.— Distribution of sources with Galactic latitude, distance, polarization degree and extinction. In the top panel, the number of stars in the two central bins are displayed beside them as they are far above the plotted range.

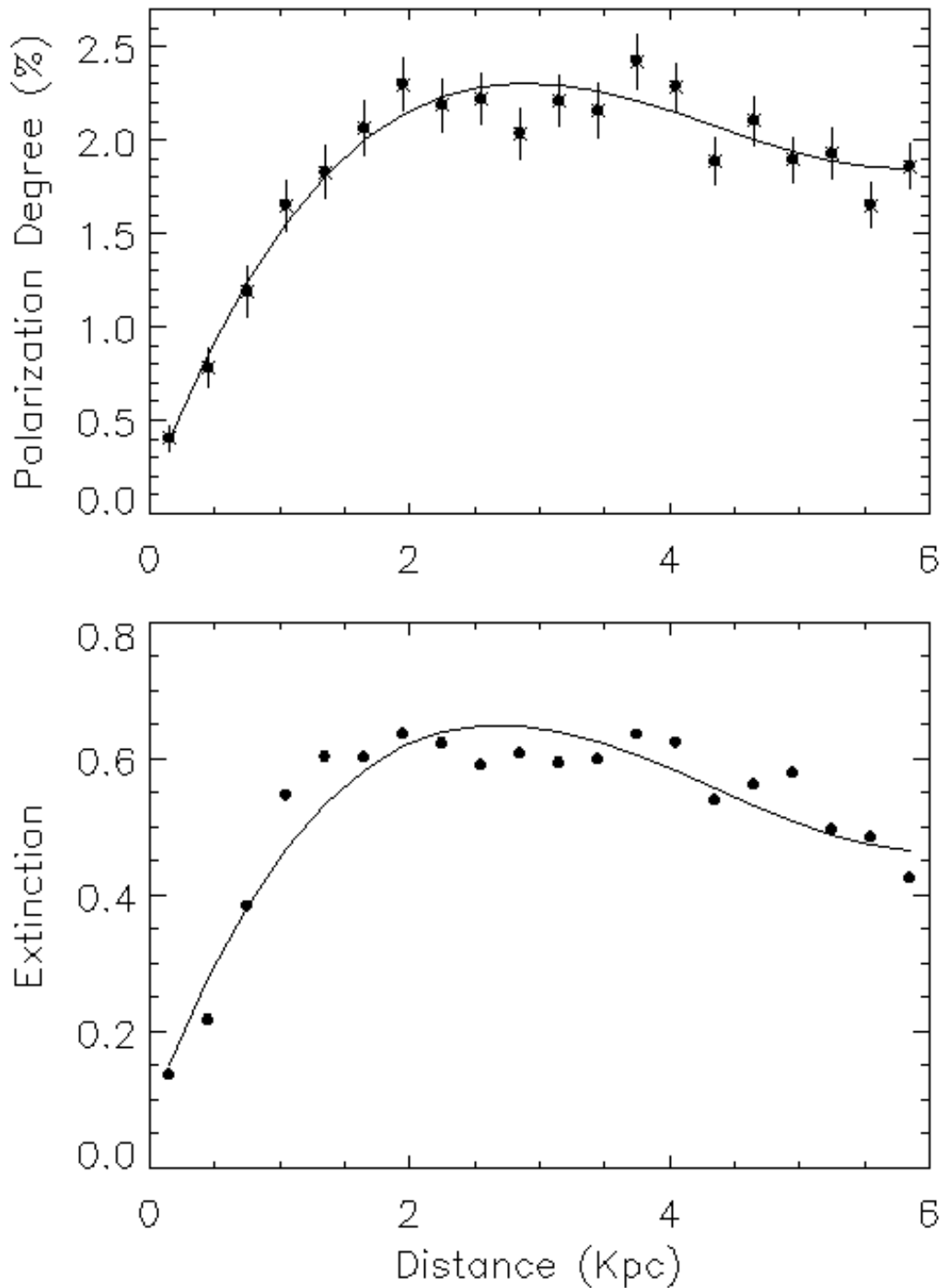


Fig. 3.— Polarization degree with (quoted) error bars (top panel) and extinction (bottom panel) in linear distance bins. Solid lines show best fit curves to third order polynomials, Eqs(1) & (2).

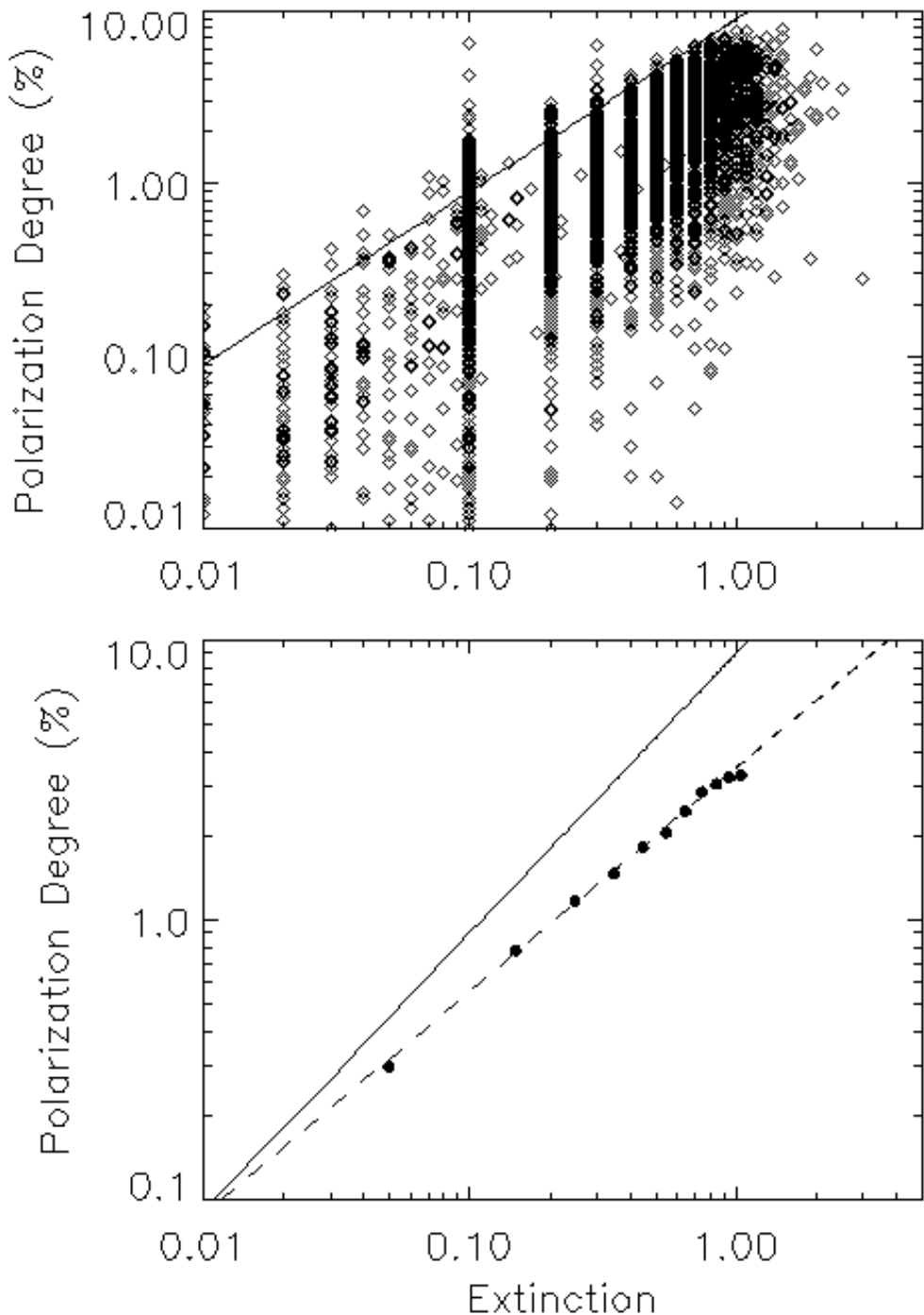


Fig. 4.— Correlation between polarization degree $P(\%)$, and extinction $E(B-V)$. Upper panel shows all individual sources while lower panel displays data averaged in extinction bins. Solid line shows the theoretical upper limit, $P(\%) = 9 E(B-V)$, for completely aligned grains by external (regular) magnetic fields. Dashed line in lower panel shows $P(\%) = 0.39 E(B-V)^{0.8}$, which is a good fit to the data up to $E(B-V) \approx 1$.

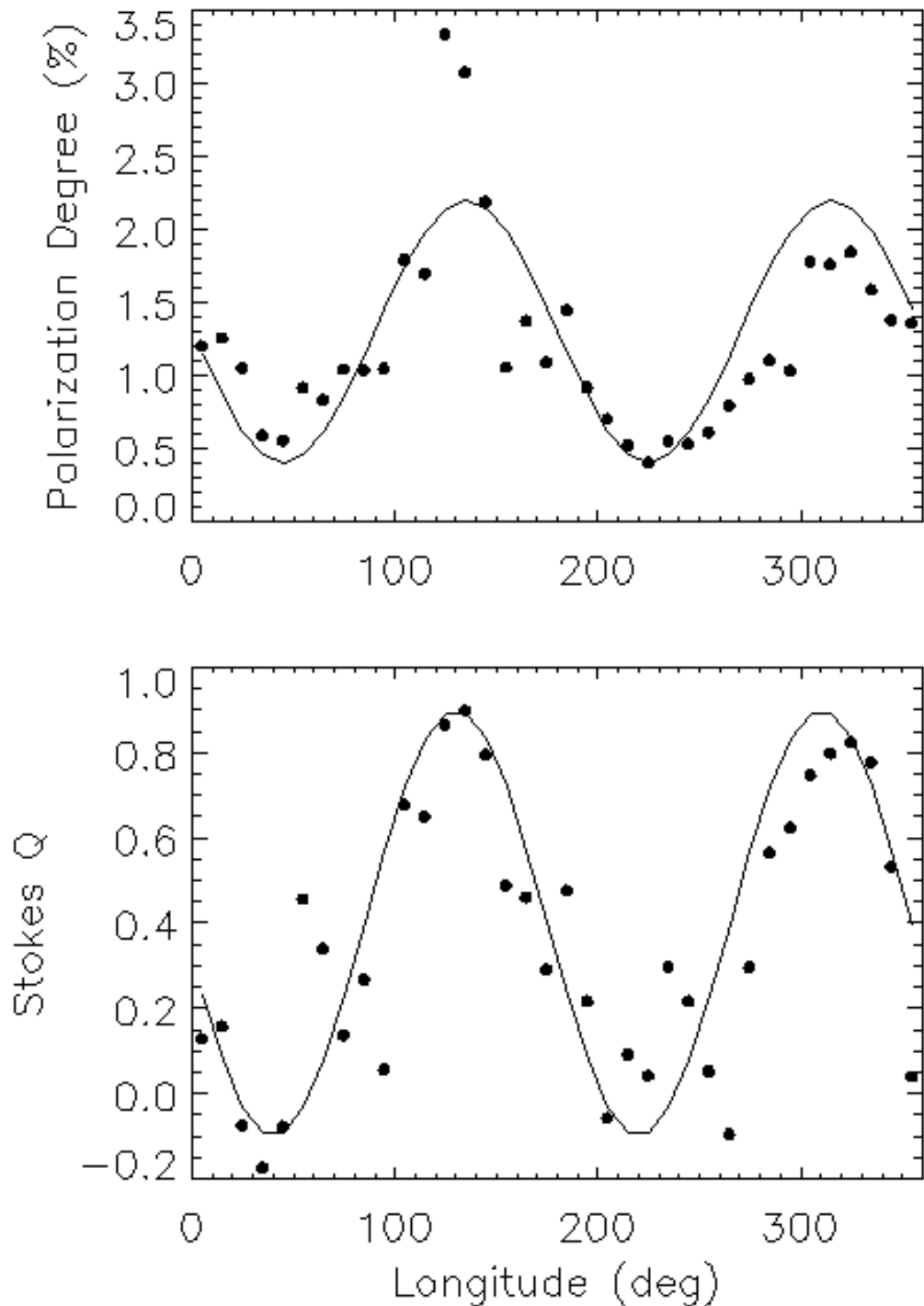


Fig. 5.— Starlight Polarization Degree (top panel) and Stokes Q parameter (bottom panel) for data averaged in 10° longitude bins. The solid line shows a best fit to a sinusoidal dependence, Eqs(5) & (6).

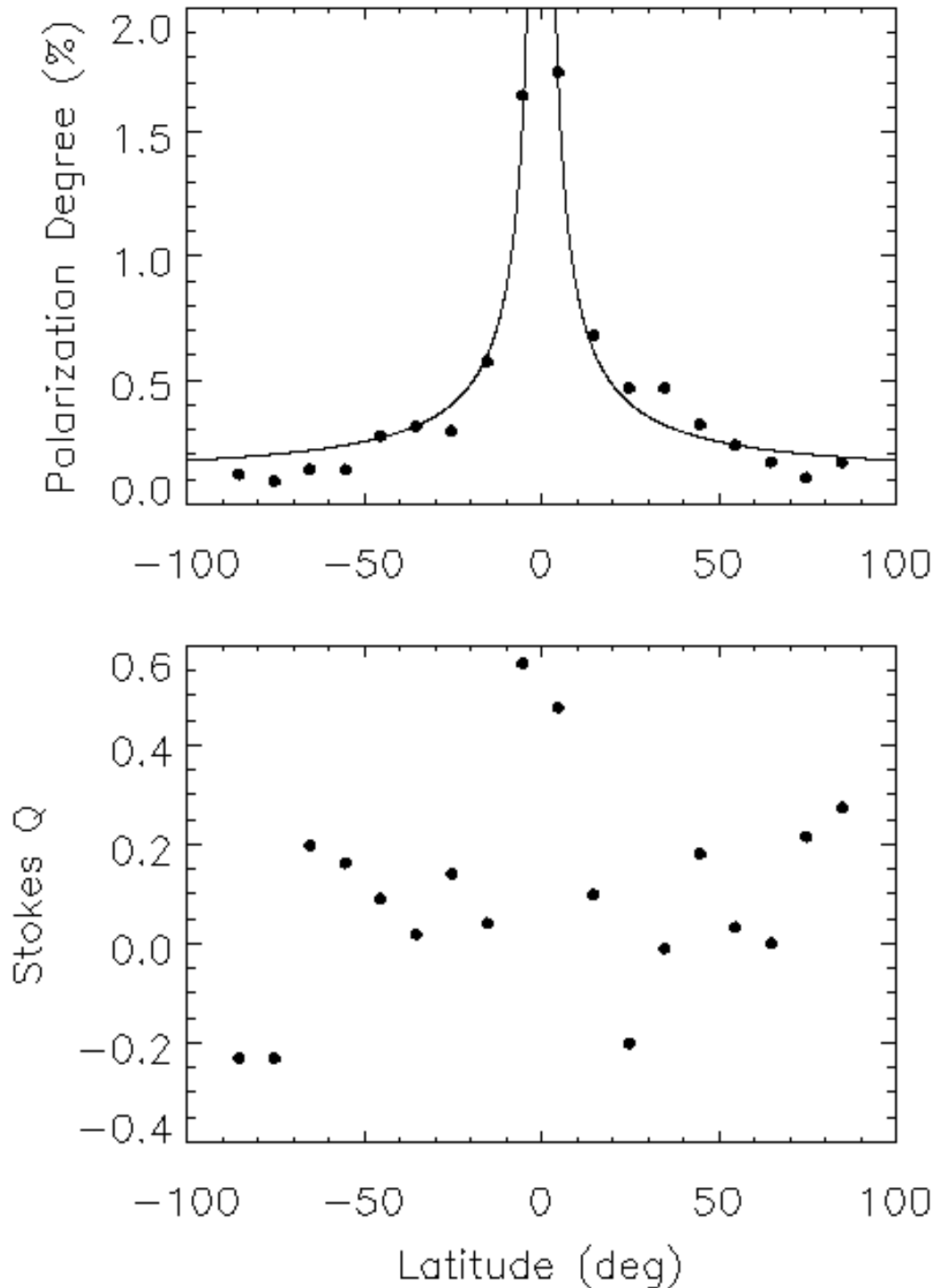


Fig. 6.— Starlight Polarization Degree (top panel) and Stokes Q parameter (bottom panel) for data averaged in 10° latitude bins. The solid line in the upper panel shows a co-secant law distribution, Eq(7).

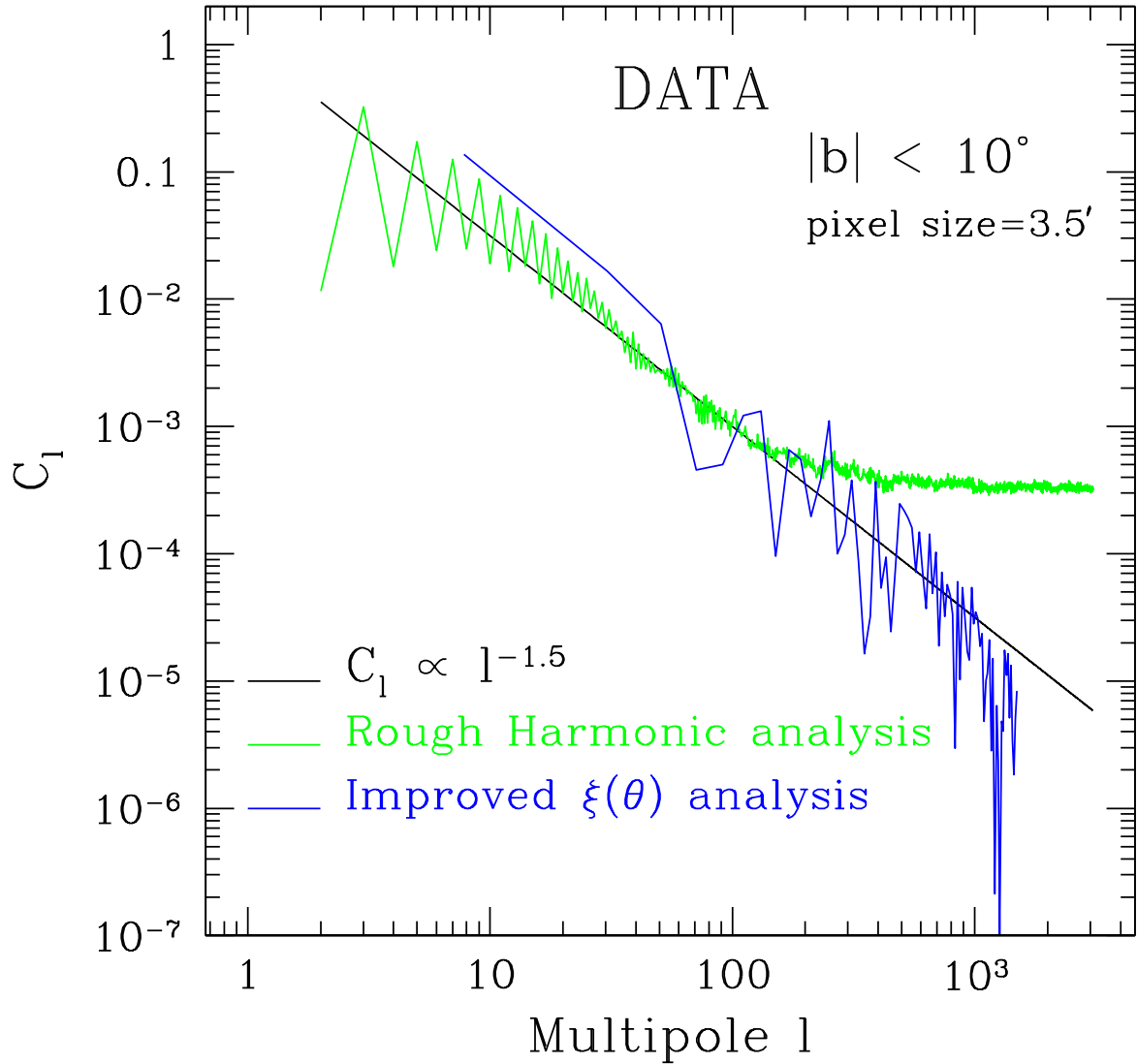


Fig. 7.— Angular power spectrum (PS) of the starlight polarization degree map in the Galactic plane, $|b| < 10^\circ$, which contains 4114 lines of sight. The PS estimation from the rough harmonic analysis (green line) is dominated by shot-noise for multipoles $\ell \gtrsim 100$ i.e, angular scales $\theta \lesssim 2^\circ$. The improved correlation function analysis (blue line), which corrects for shot-noise and pixel window effects, shows that the underlying continuum signal can be well-fitted by $C_\ell \propto \ell^{-1.5}$ (black line) down to multipoles $\ell \approx 1000$ i.e, scales $\theta \approx 10'$.

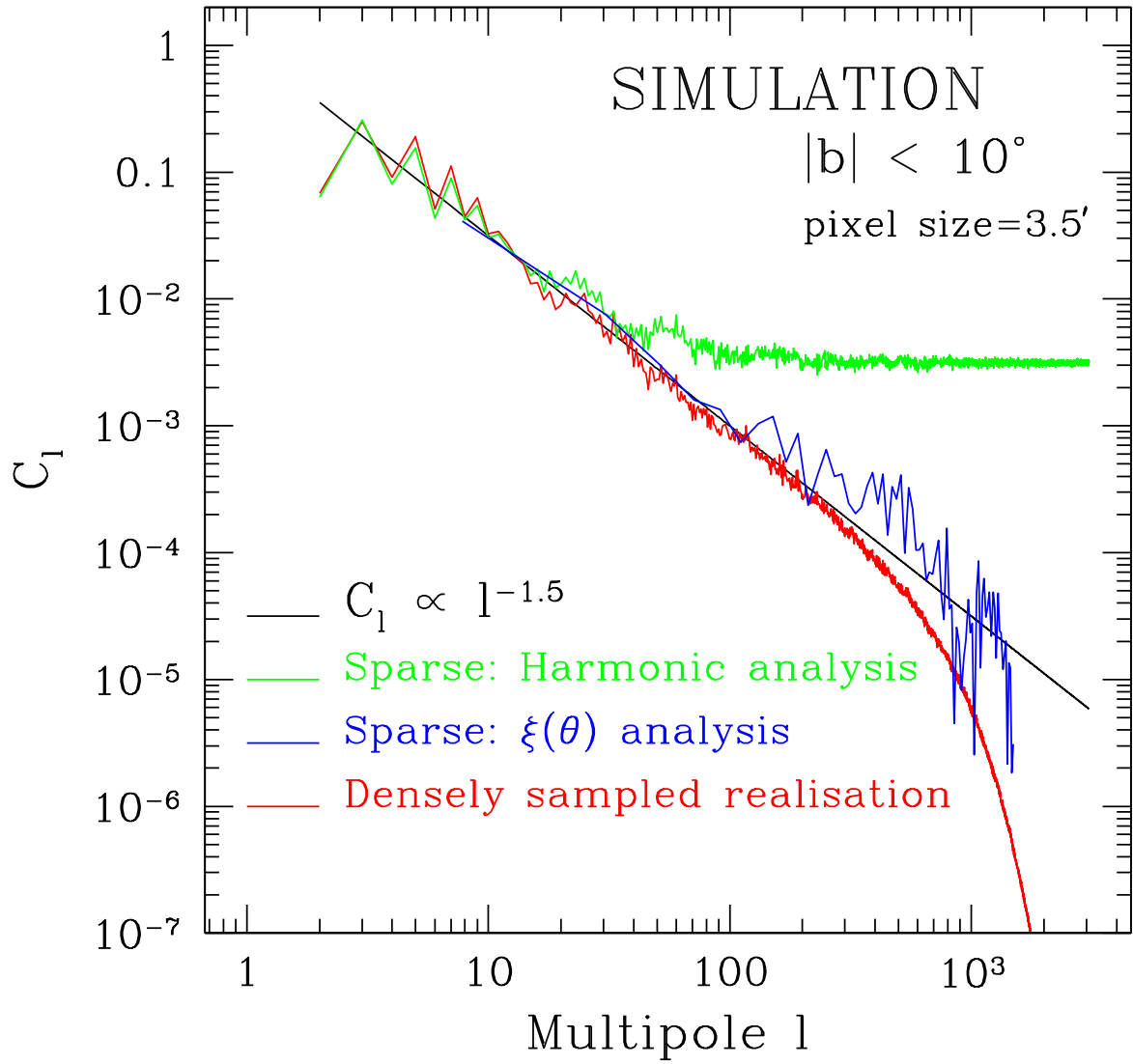


Fig. 8.— Same as Fig 7 but for the *simulated* starlight polarization degree map. The red line shows the densely-sampled (homogeneous) random-Gaussian realization of $C_\ell \propto \ell^{-1.5}$. The damping tail for $\ell \gtrsim 200$ is due to the pixel window. The PS estimation from the rough harmonic analysis (green line) is dominated by shot-noise for multipoles $\ell \gtrsim 40$ i.e, scales $\theta \lesssim 5^\circ$, while the improved correlation function analysis shows that the underlying continuum signal can be recovered down to multipoles $\ell \approx 1000$ i.e, up to scales $\theta \approx 10'$.

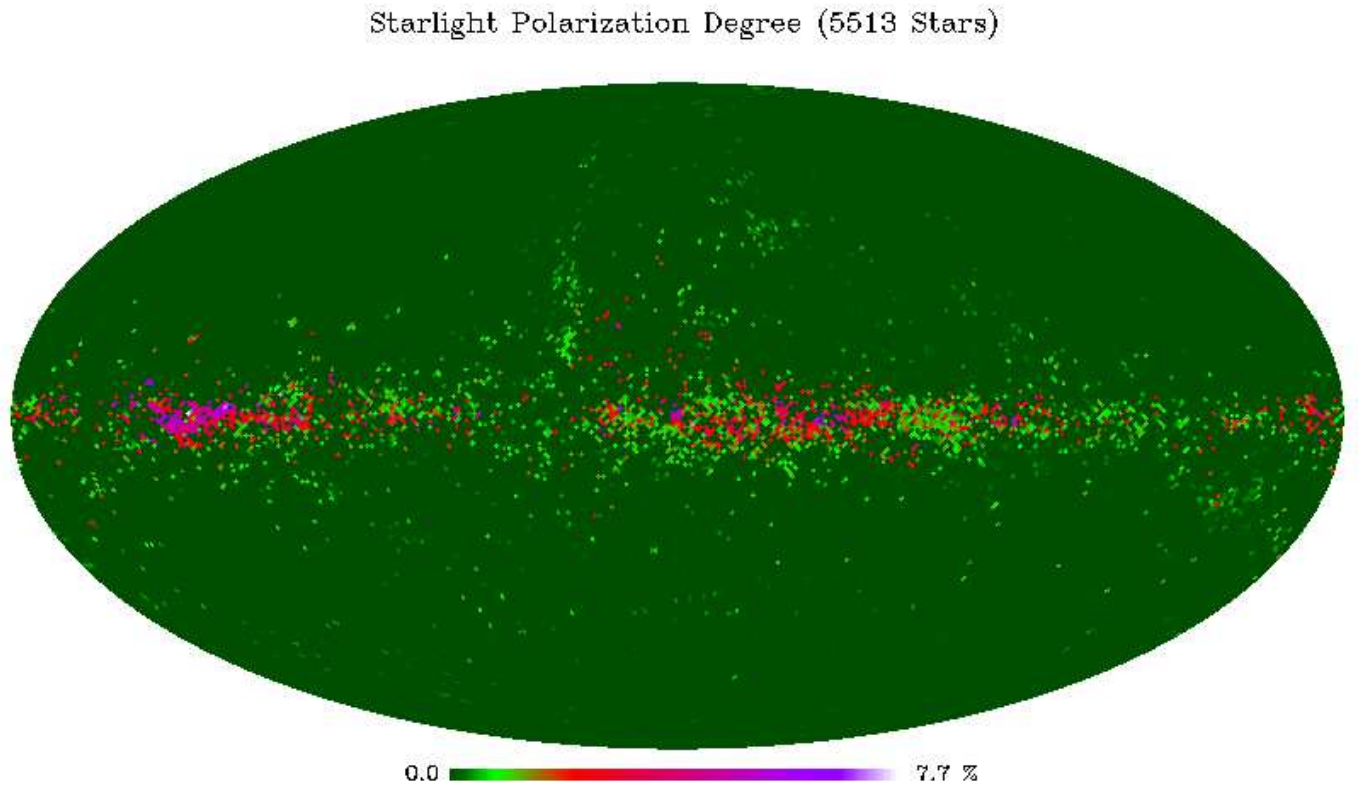


Fig. 9.— Starlight Polarization Degree for the subsample of 5513 stars in Galactic coordinates. The map is shown in HEALPix tessellation with a pixel resolution of 1° for convenience. Nearby stars (light-green sources) lie mainly at high Galactic latitudes while distant stars (red-purple sources) are found in the Galactic plane.

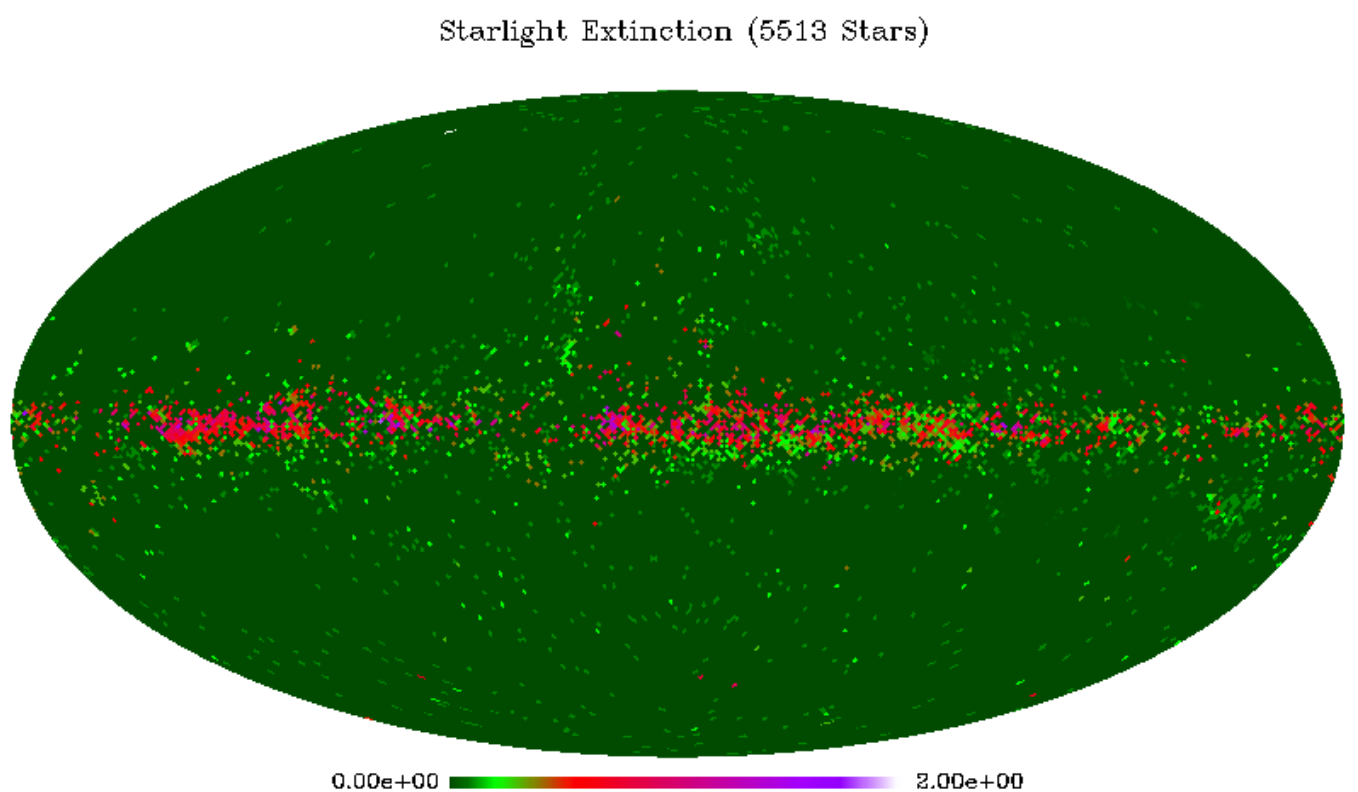


Fig. 10.— Same as Fig 9 but for Starlight Extinction, $E(B-V)$. Sources with extinction $E(B-V) > 2$ are not shown for clarity. A strong spatial correlation with the polarization degree distribution, Fig 9, is observed.

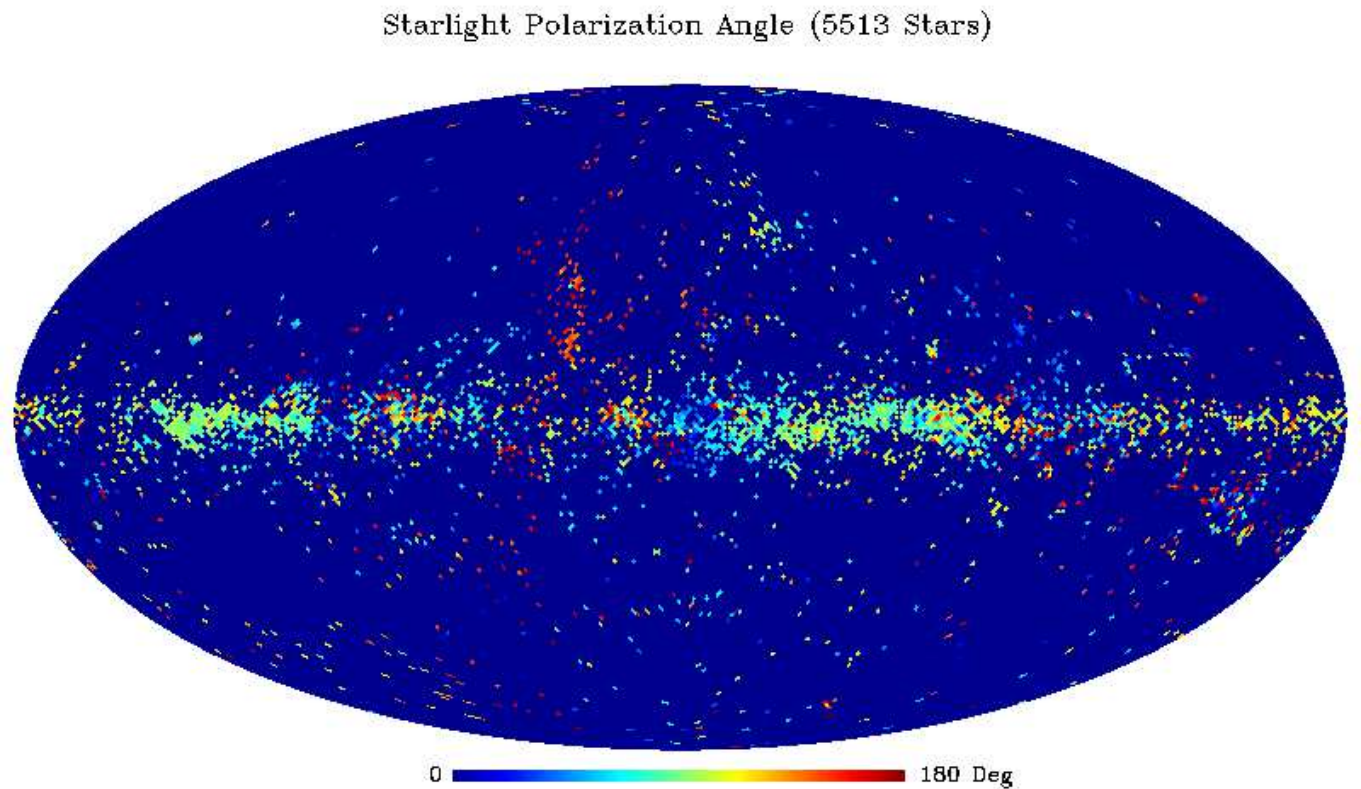


Fig. 11.— Same as Fig 9 but for the Starlight Polarization Angle. Note that, on large-scales, the polarization vectors are mostly aligned with the Galactic plane structure (light-green, light-blue and yellow sources) except for the spherical shell of Loop 1, where polarization vectors are roughly perpendicular to the Galactic plane (red sources).